The specific capacitance of Nb/Al-AlO_x/Nb SIS junctions with extremely low R_nA product

P. Yadranjee Aghdam*, Hawal Rashid, Alexey Pavolotsky, Vincent Desmaris, Victor Belitsky
Department of Earth and Space Sciences, Chalmers University of Technology, Gothenburg 41296, Sweden
*Contact: parisa.aghdam@chalmers.se

Abstract— This paper provides new insight regarding the specific capacitance of Nb/Al-AlO_x/Nb SIS junctions with low R_nA product. Employing the direct junction capacitance measurement method, the specific capacitance (C_s) and R_nA of several junctions with various R_nA values ranging from 8.8 to 68 Ω.µm^2 was studied. We noticed non-negligible scatter in the measured R_nC (normal resistance times junction capacitance) product for the junctions with the same R_nA value. We demonstrated that the local variations in the thickness distribution of the tunnel barrier could have resulted in the scatter of the R_nC data. We also show that, even at such low microwave frequencies as in our direct measurement method, the previously neglected nonlinear susceptance should be accounted, especially for junctions with low R_nA values. We present the measured C_s vs R_nA data for Nb/Al-AlOx/Nb junctions.

INTRODUCTION

The ever growing need for having wider RF and IF bandwidth in radio astronomical receiver sets stringent requirements on the SIS junction properties such as having extremely low R_nA (< 20 Ω.µm^2) values and submicron area of the device. The junction capacitance affects both the RF and IF bandwidth of SIS mixers and plays a crucial role in designing tuning circuitry [1]. At low R_nA values, the accurate value of the junction capacitance cannot be ascertained mainly due to the disagreement among the previous indirect measurements of the specific capacitance (C_s) reported in the literature [2]–[4]. In order to achieve improved accuracy compared with the previous methods, we presented a direct microwave measurement method employing a dedicated cryogenic calibration technique [5]. Our method with uncertainties down to ±2%, has an advantage over the previously used approaches, which for instance, involved extraction of the SIS junction capacitance from model of a complex superconducting resonant structure.

In this paper, great care was taken to extract the true geometrical junction capacitance. It was found that even at such low frequencies (f = 4 GHz), the susceptance [6], [7] obtained by the Kramers-Kronig transformation of the imaginary part of the response function (i.e. quasiparticle dc IV characteristics), should be calculated and subtracted from the measured capacitance. Interestingly, we found that this susceptance, which hereafter will be referred to as the nonlinear susceptance, is significant for junctions with low R_nA values. Additionally, the scatter in C_s resulted from the effect of local non-uniformities in the tunnel barrier [8] should also be considered while determining the junction capacitance. Employing the direct method in this study and extracting the true geometrical specific capacitance, the C_s vs R_nA data is obtained.

EXPERIMENT AND RESULTS

We fabricated 34 Nb/Al-AlO_x/Nb SIS junctions with R_nA and junctions' nominal areas range of 8.8–68 Ω.µm^2 and 3.6–20 µm^2, respectively. The details of the trilayer deposition parameters and the junction fabrication process are available in [5], [9]. The range of AlO_x oxygen exposure parameter for these junctions was 1530–13000 Pa.s, which is presented in details for each batch of junctions in our recent publication [8]. In order to obtain the R_nA value, the true junction size (A) (which accounted for the dimension variation due to the fabrication process) was estimated and the junction normal resistance R_n was extracted as explained in [5], [8]. The complex impedance of these junctions were directly measured at 4 GHz center frequency and at 4 K temperature. The calibration at 4 K was performed using the time-domain processing techniques and the gap voltage biased junction as the short-circuit reference [5], [10]. Then an Agilent ADS equivalent circuit model [5] was used in which the model parameters were adjusted based on the calibration. Later the SIS junction capacitance was extracted once the best fit was achieved between the model and the experimental data. More details on this procedure can be found in [5].

The measured junction capacitances (C_m) for the batch with R_nA=9.4 Ω.µm^2 are presented in Figure 1 and Figure 2. In this study, we calculated the contribution of the reactive component of the tunneling current, which results from the extreme nonlinearity of this dc I-V relation at the gap voltage [6], [7]. The resulted nonlinear susceptance calculated through the Kramers-Kronig transform of the dc I-V curve [6], [7] was capacitive under our measurement conditions [11] and was non-negligible even at such low operating frequencies (e.g. C_n in Figure 1). As can be seen in Figure 1, at low R_nA values, C_n is comparable to the C_m. More details regarding the nonlinear capacitance calculation and its important contribution can be found in [6], [7], [11]–[13]. It should be noted that the nonlinear capacitance was found to be more significant for junctions with low R_nA values [11]. Also, for junctions with the same R_nA, C_n

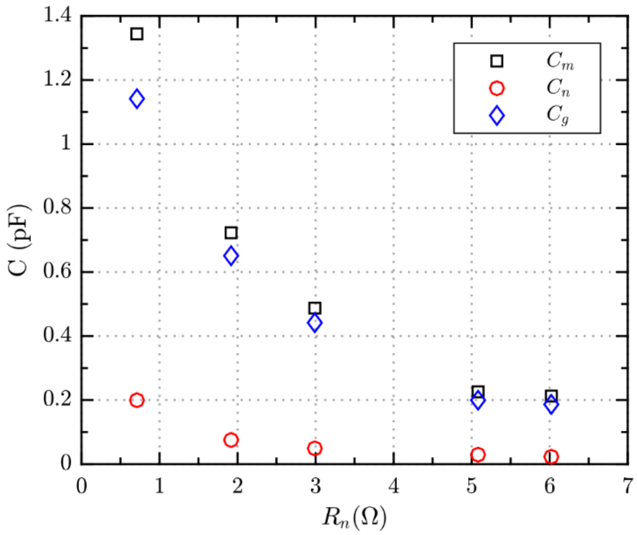

Fig. 1. The calculated nonlinear capacitance C_n (red circles) and the measured capacitance C_m (black squares) for the batch with R_nA of 9.4 $\Omega.\mu m^2$. The blue diamond data points represent the true geometrical capacitance C_g, which is obtained by the difference of C_m and C_n for each R_n. Graph is reproduced from [11].

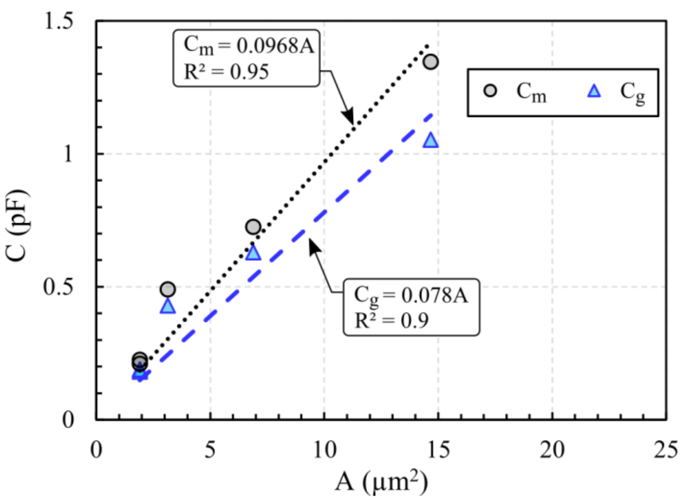

Fig. 2. The measured (C_m) and the true geometrical capacitance (C_g) as a function of the estimated area (A). From the slope of the linear fit to the C_m and C_g, the resulting specific capacitance values are obtained. Graph is reproduced from [11] .

was higher for those with lower R_n (see Figure 1). The true geometrical capacitance (C_g in Figure 1) was then obtained by subtracting the C_n from C_m. The measured and the true geometrical junction capacitances as a function of the estimated junction area (A) are presented in Figure 2. The specific junction capacitance is the slope of the fitted lines to the C (A) data points. As can be seen, the true geometrical junction capacitance results in a lower junction specific capacitance.

In [8], we investigated the origin of the scatter of the area-independent R_nC_g product (see Figure 3). We found that the scatter of as much as 40% could not only be attributed to the area estimation and the measurement uncertainty of the R_nC_g, which varies depending on the junction area and is

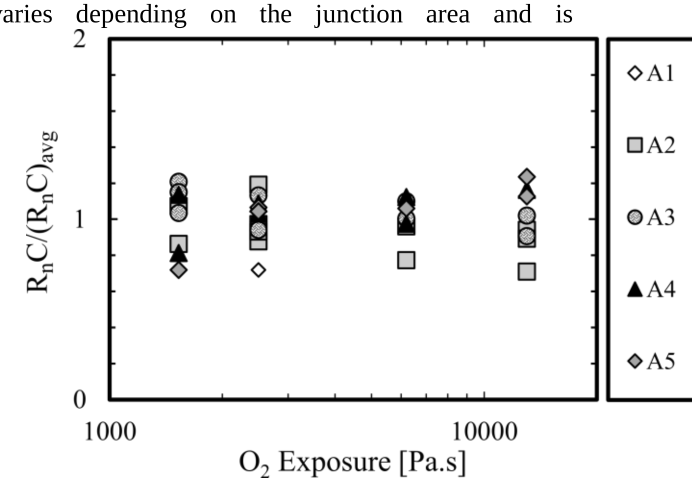

Fig. 3. $R_nC_g/(R_nC_g)_{avg}$ as a function of O_2 exposure for all the characterized junctions with areas ranging from A1=3.6 μm^2 to A5=20 μm^2, after [8].

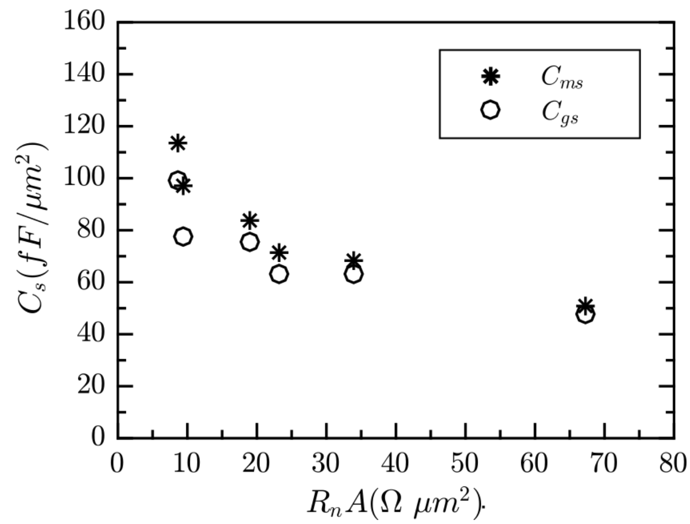

Fig. 4. The measured (C_{ms}) (asterisk) and the corrected (C_{gs}) (circle) specific capacitance as a function of R_nA. Graph is reproduced from [11]

between just ±2% to ±11.2% for the largest and smallest junctions among all the batches, respectively. Employing an illustrative model [8] and the obtained local thickness distribution of the AlO_x tunnel barrier in Nb/Al-AlO_x/Nb trilayer (using high resolution transmission electron microscopy) we demonstrated that these variations in the thickness distribution of the tunnel barrier result in the scatter of the R_nC_g data, which is consistent with our measurements. It should be noted that the scatter of the R_nC translates into the scatter in both specific capacitance and R_nA. The "local" nature of such variations over the wafer area states that averaging out the effect of these non-uniformities in junction parameters, R_nC, specific capacitance, and R_nA is less probable at the junction size scaled down. Also, such variations could be different depending on the trilayer deposition system, and hence resulting in different reports of the specific capacitance for the same R_nA [11].

The data of the measured (C_{ms}) and the true geometrical specific capacitance (C_{gs}) as a function of the R_nA value for each batch is illustrated in Figure 4. The obtained C_{gs} (R_nA) data is compared with the previously reported experimentally obtained relations in [11]. Reference [11], also proposes an improved and more accurate model for the C_s (R_nA) relation, which can greatly improve the performance of SIS mixers.

CONCLUSIONS

In this paper, the results of the directly measured junction capacitance of 34 Nb/Al-AlO_x/Nb SIS junctions with various oxygen exposure parameters were considered. It was shown that the nonlinear capacitance obtained from the Kramers-Kronig transform of the dc I-V curve is significant for junctions with low R_nA even at frequencies of a few GHz. The resulting C_{gs} (R_nA) relation was presented. Our findings show that for junctions with low R_nA values and submicron area, the scatter of C_s as a result of local thickness non-uniformities becomes more significant and should be considered.

REFERENCES

[1] A. R. Kerr, “Some fundamental and practical limits on broadband matching to capacitive devices, and the implications for SIS mixer design,” *IEEE Trans. Microw. Theory Tech.*, vol. 43, no. 1, pp. 2–13, 1995.

[2] H. S. J. van der Zant, R. a. M. Receveur, T. P. Orlando, and a. W. Kleinsasser, “One-dimensional parallel Josephson-junction arrays as a tool for diagnostics,” *Appl. Phys. Lett.*, vol. 65, no. 16, p. 2102, 1994.

[3] M. Maezawa, M. Aoyagi, H. Nakagawa, I. Kurosawa, and S. Takada, “Specific capacitance of Nb/AlOx/Nb Josephson junctions with critical current densities in the range of 0.1–18 kA/cm2,” *Appl. Phys. Lett.*, vol. 66, no. 16, p. 2134, 1995.

[4] D. M. J. Lea, “Integrated test structures for characterization of thin films for superconductor-insulator-superconductor devices and circuits,” Univ. Virginia, 1996.

[5] P. Y. Aghdam, H. Rashid, A. Pavolotsky, V. Desmaris, D. Meledin, and V. Belitsky, “Direct Measurement of Superconducting Tunnel Junction Capacitance,” *IEEE Trans. Terahertz Sci. Technol.*, vol. 5, no. 3, pp. 464–469, May 2015.

[6] J. Tucker and M. Feldman, “Quantum detection at millimeter wavelengths,” *Rev. Mod. Phys.*, vol. 57, no. 4, pp. 1055–1113, Oct. 1985.

[7] H. Rashid, V. Desmaris, A. Pavolotsky, and V. Belitsky, “Harmonic and reactive behavior of the quasiparticle tunnel current in SIS junctions,” *AIP Adv.*, vol. 6, no. 4, p. 45109, Apr. 2016.

[8] P. Yadranjee Aghdam, H. Marouf Rashid, A. Pavolotsky, V. Desmaris, and V. Belitsky, “Dependence of the scatter of the electrical properties on local non-uniformities of the tunnel barrier in Nb/Al-AlOx/Nb junctions,” *J. Appl. Phys.*, vol. 119, no. 5, p. 54502, Feb. 2016.

[9] A. B. Pavolotsky, D. Dochev, and V. Belitsky, “Aging- and annealing-induced variations in Nb/Al–AlOx/Nb tunnel junction properties,” *J. Appl. Phys.*, vol. 109, no. 2, p. 24502, 2011.

[10] H. Rashid, D. Meledin, V. Desmaris, A. Pavolotsky, and V. Belitsky, “Superconducting 4–8-GHz Hybrid Assembly for 2SB Cryogenic THz Receivers,” *IEEE Trans. Terahertz Sci. Technol.*, vol. 4, no. 2, pp. 193–200, Mar. 2014.

[11] P. Yadranjee Aghdam, H. Rashid, A. Pavolotsky, V. Desmaris, and V. Belitsky, “Specific Capacitance Dependence on the Specific Resistance in Nb/Al-AlOx/Nb Tunnel Junctions,” *Submitt. to IEEE Trans. Terahertz Sci. Technol.*, 2017.

[12] H. Rashid, S. Krause, D. Meledin, V. Desmaris, A. Pavolotsky, and V. Belitsky, “Frequency Multiplier Based on Distributed Superconducting Tunnel Junctions: Theory, Design, and Characterization,” *IEEE Trans. Terahertz Sci. Technol.*, vol. 6, no. 5, pp. 1–13, 2016.

[13] H. Rashid, V. Desmaris, A. Pavolotsky, and V. Belitsky, “THz Frequency Up-Conversion using Superconducting Tunnel Junction,” *IEEE Microw. Wirel. Components Lett.*, vol. 26, no. 10, pp. 831–833, Oct. 2016.

.